Excitonic Pathway to Photoinduced Magnetism in Colloidal Nanocrystals with Nonmagnetic Dopants

Valerio Pinchetti[1], Qiumei Di[2], Monica Lorenzon[1], Andrea Cammellini[3], Mauro Fasoli[1], Margherita Zavelani-Rossi[3], Francesco Meinardi[1], Jiatao Zhang[2*], Scott A. Crooker[4*], Sergio Brovelli[1]*

[1] *Dipartimento di Scienza dei Materiali, Università degli Studi di Milano-Bicocca, via Roberto Cozzi 55, I-20125 Milano, Italy*
[2] *Research Center of Materials Science, School of Materials Science and Engineering, Beijing Institute of Technology, Beijing 100081, P.R. China*
[3] *Dipartimento di Fisica, Politecnico di Milano, Piazza Leonardo da Vinci 32, IT-20133 Milano, Italy*
[4] *National High Magnetic Field Laboratory, Los Alamos, New Mexico 87545, United States*

*e-mail: sergio.brovelli@mater.unimib.it; crooker@lanl.gov; zhangjt@bit.edu.cn

'Electronic doping' of colloidal semiconductor nanostructures through controlled incorporation of metal impurities, aliovalent with respect to the cation sub-lattice, holds promise for future design of functional nanomaterials and advanced device concepts in optoelectronics, photonics and spin-based technologies. An emerging electronic dopant in III-V and II-VI nanostructures is silver, whose incorporation as Ag^+ impurity leads to the introduction of intragap electronic states and the development of a largely Stokes-shifted emission resulting from an optical transition coupling the host conduction band to the dopant 4*d* states. Having a full *d* electronic shell, Ag^+ is nominally nonmagnetic and luminescence is often ascribed to transfer of the photoexcited hole from the host valence band to the Ag^+ site, which then behaves as a radiative acceptor centre for a conduction band electron. The mechanism of this optical-activation process and, specifically, the associated modification of the electronic configuration of the Ag ion remain unclear. Here we combine site-selective photoluminescence and transient transmission experiments with spectro-electrochemical methods and magnetic circular dichroism spectroscopy to trace a comprehensive picture of the dopant-mediated excitonic process in Ag-doped CdSe nanocrystals. Our results demonstrate that, in contrast to expectations based on silver ionization energy and Jan-Teller crystal effects, hole-capture effectively leads to transient conversion of Ag^+ to paramagnetic Ag^{2+}-like species. This results in strong optically-activated magnetism and diluted magnetic semiconductor behaviour, demonstrating that optically switchable magnetic nanomaterials can be obtained by exploiting the excitonic processes involving nominally nonmagnetic impurities.

Colloidal semiconductor nanocrystals (NCs) are solution processable functional materials with tunable electronic properties[1,2] that are receiving growing attention in several optoelectronics and photonic technologies, including solid state lighting,[3,4] lasing,[5] photovoltaics,[6] photodetection,[7] sensors,[8] bio-labels[9,10] and, more recently, luminescent solar concentrators.[11-16] In addition to size-control[17,18] and heterostructuring[19] providing spectral tunability and control over the exciton dynamics,[20,21] the intentional insertion of tiny amounts of transition metal ions, also referred to as doping,[22,23] is an effective strategy for achieving broadband, largely Stokes-shifted luminescence[24-32], enhanced electrical transport[33,34] and tailored magnetic behaviours arising from the *sp-d* spin-

exchange interaction between the NC quantized states and the *d*-electrons of the impurity atom.[25,32,35-37] Doping chalcogenide NCs with manganese[38] has been particularly extensively investigated for applications in magnetic memory and spin-based electronics.[39-44] Because Mn^{2+} ions are isovalent to the lattice cations, their substitutional incorporation in II-VI NCs introduces no additional charge in the system. For small, wide-band-gap NCs (E_g>2.1 eV), the Mn *d*-states behave as localized radiative recombination centres for band-edge excitons, resulting in the typical Mn^{2+} luminescence at ~2.1 eV sensitized by the host particle,[38] while for larger NCs (E_g<2.1 eV), the unpaired electronic spins of the Mn-ions interact with photogenerated[45] and electrically injected[46] excitons to form magnetic polarons. Conversely, copper and silver ions introduce a single intragap deep acceptor level close to the host valence band (VB),[47-50] which radiatively captures conduction band (CB) electrons,[28,30,33,51-53] making the dopant-related emission subject to quantum confinement[54,55] and heterostructuring.[52] Furthermore, being aliovalent with respect to cations in II-VI and III-V semiconductors, their insertion changes the overall charge within the host compound, resulting in *p*- or *n*- type doping depending on their coordination state.[33,34,52,53,56-59] For this reason, they are commonly labelled as *electronic dopants*. In the case of silver-doped NCs, electric transport measurements on Ag:CdSe NCs by Norris and co-workers reported that, in the low doping regime (<1%), Ag atoms incorporate as interstitial impurities, whereas for higher doping levels they occupy substitutional cation sites, respectively leading to *n*- or *p*-type transport[33,60-62]. Consistently, Kang *et al*[34] observed *p*-type transport in field effect transistors incorporating PbSe NCs with relatively high Ag doping level and scanning tunnel spectroscopy by Mocatta *et al*[58] showed the Fermi level (FL) of heavily doped Ag:InAs NCs close to the VB onset. Recent density functional theory calculations of the electronic structure of Ag:CdSe NCs (3.9% Ag) predicted a deep acceptor state close to the NC valence band with optical behaviour similar to the acceptor state in NCs with Cu^{+} impurities, yet with a more pronounced *s*-character deriving from the coordinating Se anions.[53]

Despite silver and copper belonging to the same group of the periodic table, their electronic properties show fundamental differences arising from the interplay between their second ionization (IE_2) and crystal field stabilization energies. In the case of Cu (atomic radius r_0=1.35Å),[63] the enhanced stability due to tetragonal distortion of the local environment (i.e. host lattice or molecular ligands) of Cu^{2+} compensates the energy required to form a doubly-charged ion (IE_2^{Cu}=20.29eV).[64] This results in the amphoteric character of Cu dopants, which exhibit stable oxidation states +1 or +2 depending on the position of the Fermi energy.[28,49,50,65] Silver, on the other hand, is energetically less sensitive to the breakdown of local symmetry due to its ~20% larger atomic radius (1.60Å)[63] with respect to copper, making its crystal field stabilization energy typically insufficient to counterbalance its larger second ionization energy (IE_2^{Ag}=21.45eV).[64,66-69] As a result, silver cations assume almost exclusively the +1 oxidation state, whereas stable +2 configuration is found in rare compounds where Ag^{2+} ions are protected against reduction by suitable ligands.[64,70-73] Consistently, in bulk metal chalcogenides, silver atoms are inserted as nonmagnetic +1 impurities[74] with electronic configuration [Kr]4d^{10}, often coupled to a compensating defect ensuring charge neutrality.[47,75,76] Having a full *d*-shell, luminescence in Ag-doped systems requires transfer of the photoexcited hole from the host VB to the Ag^+ site, which then behaves as radiative acceptor centre for a CB electron.[30,53,67,75,77] Similarly, Cu^+ centers are not magnetic (there is no unpaired electron spin in their full 3*d* shell) and are optically passive; capture of a VB hole is necessary to promote them to Cu^{2+} with electron-accepting capability and thereby activate the Cu-related luminescence.[28,51] For lower Fermi energies, the oxidation state of Cu becomes +2 (electronic configuration [Ar]3d^9): The 3*d* shell now contains one unpaired electron and therefore exhibits paramagnetic character and holelike behaviour, resulting in the characteristic Cu-luminescence without the explicit need for a photogenerated VB hole.[50,52] Spectro-electrochemistry experiments[28] corroborated by spectroscopic measurements in the presence of a hole-scavenging Lewis base,[52,57] indicated that the emission efficiency of copper-doped NCs is unaffected by ultrafast trapping of the VB hole, suggesting a dominant role of substitutional Cu^{2+} centres in the emission process. In support of this picture, magnetic circular dichroism studies on the

same Cu:ZnSe NCs revealed a significantly enhanced and strongly temperature-dependent Zeeman splitting of the 1S exciton, indicating *sp-d* exchange coupling between the 1S exciton to paramagnetic spins in the NC - a defining characteristic of diluted magnetic semiconductors (DMS).[29] Surprisingly, the paramagnetism of Cu-doped NCs was observed to be strongly intensified by UV illumination. This was ascribed to the rapid localization of the VB hole at the nonmagnetic Cu^{+} making it formally Cu^{2+}-like and thereby increasing the number of paramagnetic centres in a NC.[29]

This result brought into focus the idea that optically-switchable magnetism can be obtained by exploitation of excitonic mechanisms in nanostructures doped with nominally nonmagnetic dopants, such as silver. To date, however, such concept has not yet been realized and a comprehensive picture of the photophysical and magnetic phenomena in Ag-doped NCs is still lacking. In this work, we aimed to address this by combining photoluminescence (PL) and transient absorption (TA) measurements with spectro-electrochemical (SEC) methods and magnetic circular dichroism (MCD) spectroscopy on Ag-doped CdSe NCs. PL experiments in site-selective excitation conditions show, for the first time, that the Ag^{+}-related emission in Ag:NCs can be achieved both via sensitization from the NC host using above-gap excitation *and* by resonant excitation with below-gap light. This provides a first indication that the $Ag(d^{10})+h\nu \rightarrow Ag(d^{9})+e_{CB}$ transition, effectively corresponding to the transient conversion of nonmagnetic Ag^{+} to paramagnetic Ag^{2+}-like species, can be promoted optically. Accordingly, TA measurements show that both the 1S excitonic band and the sub-bandgap Ag^{+} absorption are bleached by band-edge excitation, confirming the promotion of the Ag^{+} electron to the NC CB. The different dynamics of the 1S and dopant TA signals further enables us to measure the localization time of the VB hole in Ag^{+}. SEC measurements support this picture and clarify the role of radiative and nonradiative channels in the recombination mechanism. Remarkably, temperature- and magnetic field-dependent MCD experiments show strong *sp-d* spin-exchange interactions and over 100% enhancement of the magnetic response under additional UV illumination, demonstrating the original hypothesis that ground-state nonmagnetic dopants, such as Ag^{+} in II-VI

NCs, can be used to realize photo-switchable nanostructures exhibiting paramagnetism. Time-resolved measurements finally show that the photoinduced MCD follows minutes-long dynamics that correlates well with the PL transient due to charging/discharging of the NCs, indicating that the lifetime of the metastable paramagnetic state is strongly extended by trapping of electrons.

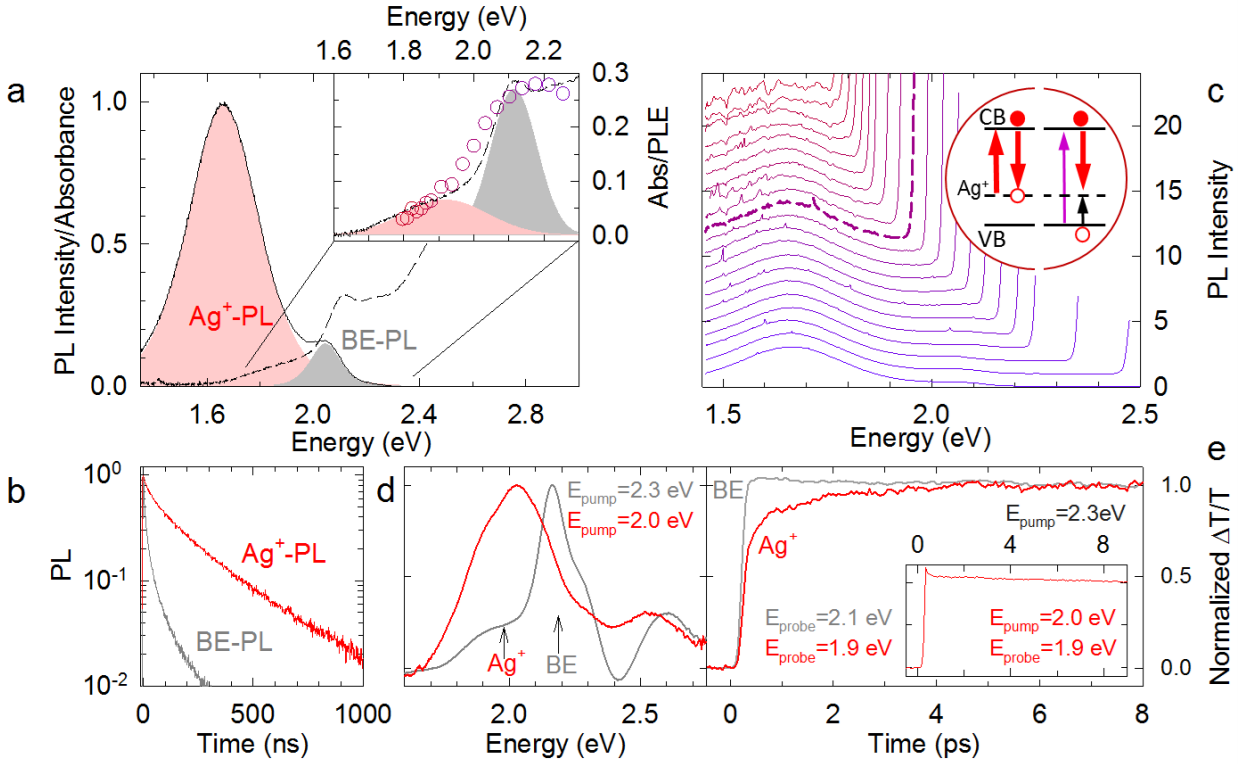

Figure 1 a. Optical properties of Ag-doped CdSe nanocrystals. Optical absorption (dashed line) and photoluminescence (PL) spectra of Ag-doped CdSe NCs (radius 2.2±0.4 nm) in toluene showing the band-edge PL band (highlighted in grey) and the dopant-related emission (red shading). The inset shows an enlargement of the 1.6-2.25 eV region emphasizing the intragap absorption band peaked at ~1.9 eV due to sub-bandgap absorption by the Ag^+ impurities (red shading) on the low-energy side of the 1S feature at ~2.1 eV (grey shading). The circles report the PL excitation (PLE) spectrum of the Ag^+-PL at ~1.65 eV. **b.** PL decay curves of the BE-PL and the Ag^+-PL measured at the respective absorption maxima using 3.1 eV excitation. **c**. PL spectra of the same NCs under progressively lower energy excitation (from bottom to top). The colour scheme is the same as the respective circle in the inset of 'a'. A portion of the excitation light is included for reference; it allows for direct comparison between the different measurements. The dashed line roughly indicates the transition between above-gap and below-excitation depicted in the right and left hand side of the scheme shown in the inset. All these measurements are performed at room temperature. **d**. Normalized transient transmission spectra after band-to-band pumping at 2.3 eV (grey curve) and intragap excitation of Ag^+ at 2.0 eV (red curve). The spectra are collected after 1.5 ps delay, in both cases the fluence is set to excite an average of 0.1 excitons per NC. **e**. Normalized bleaching ΔT/T kinetics of the 1S absorption (2.1 eV, grey line) and of the Ag^+ absorption (1.9 eV, red line) upon pumping close to the band-edge at 2.3 eV to minimize thermalization effects. The bleaching of the 1S absorption is instantaneous whereas the Ag^+ signal shows a slower rise time due to hole transfer from the VB. Inset: The kinetics of the Ag^+ bleaching becomes essentially instantaneous upon direct pumping at 2.0 eV.

Results and Discussion

Synthesis and optical properties of Ag:CdSe NCs. Silver-doped CdSe NCs with 0.3% Ag were prepared via in-situ sulfuration and cation exchange reaction of Ag nanoparticles (NPs).[56] Briefly, monodisperse Ag NPs (~5 nm) were prepared first according to Li et al.,[78] which can be further used in the preparation of amorphous Ag_2Se NPs by sulfuration with a Se precursor in the molar ratio of 1:5 at 50°C. The Se precursor was prepared from 1 mmol Se powder with 7 mL octadecylene at 270°C. The obtained Ag_2Se NCs (0.035 mmol) were dispersed in 10 mL toluene with 0.2 mL of oleic acid and 0.1 mL oleylamine. After that, 1 ml methanol solution containing 0.1 g of $Cd(NO_3)_2 \cdot 4H_2O$ was added. After 2-minutes magnetic stirring, 0.1 mL tributyl phosphate was added and the mixture was heated at 55 °C for 1 h under magnetic stirring. The compositional and structural details of the NCs, including transmission electron microscopy, X-ray diffraction analysis and X-ray photoemission spectroscopy are reported in Figures S1-S3 and Table S1, showing spherical particles with average radius of 2.2±0.4 nm in wurtzite crystal structure.

We start our analysis by looking at the absorption and PL spectra of Ag:CdSe NCs reported in Figure 1a, showing the 1S absorption peak of the CdSe host at ~2.11 eV, closely resonant to a weak band-edge emission (BE-PL) at ~2.05 eV with average lifetime of ~11 ns (Figure 1b), likely arising from a minor subpopulation of undoped NCs, in which the cation exchange reaction has led to complete substitution of Ag with Cd ions. The emission spectrum is dominated by a broadband component at ~1.66 eV with average lifetime of ~220 ns (Figure 1b) due to the radiative decay of CB electrons to the localized intragap states of silver (Ag^+-PL), Stokes-shifted by ~400 meV from the 1S absorption peak, in agreement with previous reports.[53,56,77] Notably, the absorption spectrum shows a broad low-energy component below the 1S peak extending to 1.7 eV, nearly resonant to the Ag^+-PL band. As shown in Figure 1c, by tuning the excitation energy from 3.0 eV (above CdSe bandgap) down to 1.8 eV (below NC band edge) Ag^+-PL is still observed. This indicates that the *d*-electrons of Ag^+ can be promoted to the NC conduction band by direct optical excitation using sub-band-gap excitation following the reaction $Ag(d^{10})+h\nu \rightarrow Ag(d^9)+e_{CB}$, where Ag^+ species are temporarily photoconverted

into Ag^{2+}-like centres, similar to what was observed in CdSe NCs doped with Cu^{+} species.[79] As a result, the PL excitation (PLE) spectrum of the 1.7 eV emission shown in the inset of Figure 1a resembles rather well the respective absorption profile down to sub-bandgap energies. A schematic depiction of the photophysical mechanism under either above-gap or below-gap excitation is reported in the inset of Figure 1c.

Independent confirmation of the promotion of Ag^{+} 4*d* electrons to the NC CB is provided by the TA data in Figure 1d, showing the TA spectra under BE excitation and intragap pumping of Ag^{+}. Band-edge pumping results in the typical TA spectrum of CdSe NCs, with an intense positive band at 2.2 eV corresponding to bleaching of the 1S absorption due to state filling of the double degenerate CB.[1] More importantly, the TA spectrum shows an additional positive band resonant to the Ag^{+} absorption at 1.9 eV, which is observed also under intragap pumping of Ag^{+} at 2.0 eV. This indicates that the transition of Ag^{+} centres is bleached by BE pumping, thus confirming that direct excitation of Ag^{+} with sub-band-gap light promotes its *d*-electron to the NC CB. The inspection of the time transients of the bleaching signals in Figure 1e further enables us to directly measure the hole localization time from the NC VB to the Ag^{+}. Under pumping at 2.3 eV, which is nearly resonant to the NC BE, the 1S bleaching grows with no measurable rise time, as expected in the absence of thermalization effects. In contrast, the Ag^{+} bleaching shows a markedly slower component following an initial instantaneous growth. The slow rise with time constant τ~1.4 ps (as extracted with a double exponential fit, Figure S4), is ascribed to the localization of the photoexcited hole from the NC VB to the Ag^{+}, yielding a similar TA signature as that observed for hole localization in CdSe/CdS core/shell structures upon shell excitation.[80] This interpretation is supported by the instantaneous growth of the Ag^{+} bleaching observed under direct intragap with 2.0 eV light (inset of Figure 1e), which further suggests that the fast growth of the Ag^{+} bleaching under BE pumping is likely due to direct excitation of Ag^{+} ions.

Spectroelectrochemistry experiments. To confirm the above mechanism and to clarify the nature of the intragap dopant state, we conduct, for the first time, SEC experiments on Ag-doped NCs. The

custom experimental setup is illustrated in Figure 2a that also reports a schematic depiction of the NC band structure featuring the fully occupied *d*-state of Ag^+ in the lower part of the energy gap. In unperturbed conditions, the Fermi level (FL) is tentatively placed between the Ag^+-level and the conduction band of the NC host. The intragap defect states (DS in Figure 2a) responsible for the SEC behaviour are placed in energy slightly above the FL, in agreement with the observed EC response described below. The NCs are excited with a continuous wave laser (3.1 eV excitation) and the PL is collected under the application of an EC potential (V_{EC}) that tunes the position of the FL in a controlled and reversible fashion.[28,81-84] Specifically, negative V_{EC} correspond to a raising Fermi energy and leads to progressive passivation of nonradiative traps for photoexcited electrons. Concomitantly, excess electrons accumulated in surface defects become efficient traps for photogenerated holes. Conversely, positive V_{EC} (corresponding to lowering the FL) depletes the NC of photoexcited electrons and concomitantly passivates hole trapping defect states. The total brightening versus quenching effect of V_{EC} on the NC emission efficiency is therefore determined by the competition between the selective passivation/activation of carrier traps, by the respective trapping rates and by the occupancy of the surface states in unperturbed conditions. For this reason, SEC measurements are particularly useful for identifying the trapping mechanisms that mostly affect the exciton decay and therefore can help to design specific passivation strategies for optimizing the PL yield of NCs. Furthermore, the selectivity of SEC measurements for band-edge carriers enables us to probe the nature of intragap states (i.e. donor *vs*. acceptor, both intrinsic due to points defects or introduced by doping) involved in the recombination mechanism and to reveal the sequence of events leading to radiative decay.

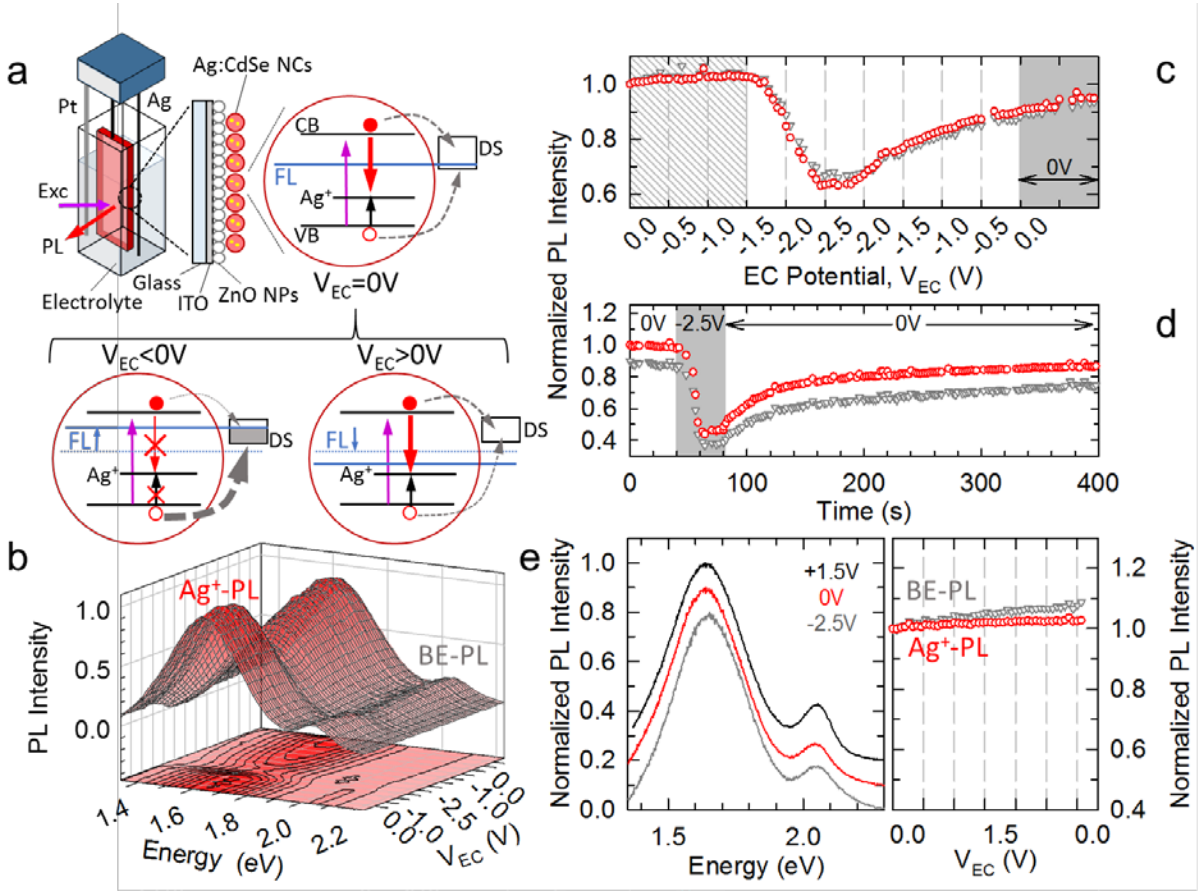

Figure 2. Spectroelectrochemistry of Ag:CdSe nanocrystals. a, Schematics of the SEC setup consisting of an EC cell with tetrabutylammonium perchlorate in propylene carbonate (0.1 M) as an electrolyte and a working electrode comprising an ITO-coated glass covered with a layer of ZnO nanoparticles (NPs) and Ag:CdSe NCs. The figure also illustrates the radiative recombination pathway (red arrow) of photoexcited conduction band (CB) electrons to the intragap Ag-state following the capture of the valence band (VB) hole (black arrow). The competitive nonradiative carrier trapping processes to defect states (DS) are shown as grey dashed arrows. The effect of the EC potential on the PL intensity depends on the filling/emptying DS (right of the band diagram) in response to changes in the position of the Fermi level (FL; blue line). **b**. A series of PL spectra (0.5 s acquisition time per frame) for a stepwise scan of the EC potential to negative values (100 mV steps each lasting 10s). **c**. Spectrally integrated intensity of the BE and Ag^+-PL bands (grey triangles and red circles respectively) as a function of V_{EC} extracted from the spectra in 'b'. The patterned area for $V_{EC} \leq 1V$ highlights the regime in which the ZnO NPs interlayer and the dielectric ligands attenuate the effect of the applied potential. The grey shaded portion emphasizes the PL growth over time at $V_{EC}=0V$. **d**. Intensity of the BE and Ag^+-PL bands (grey triangles and red circles respectively) for excitation at 3.1 eV during ON/OFF voltage cycles for the negative electrochemical potential (V_{EC} = 0, −2.5, 0 V) showing the recovery of the initial intensity due to slow release of trapped holes. **e**. Normalized PL spectra at V_{EC} = 0 V (red line), -2.5 V (grey line) and +1.5 V (black line). The spectra are shifted vertically for clarity. **f**. Spectrally integrated PL intensity during a stepwise scan of the EC potential to positive values (100 mV steps each lasting 10s). All intensities in 'c', 'd' and 'f' are normalized to their values at V_{EC} = 0 V. All measurements are conducted using 3.1 eV excitation with fluence of 100 nJ/cm^2.

We start our analysis by applying a negative V_{EC} to Ag:CdSe NCs. In Figure 2b, we report the complete set of PL spectra of the NCs under application of a negative V_{EC} scanned from 0 V to −2.5

V and then back to 0 V (100 mV potential steps, step duration 10 s). To quantify the effect of the EC potential on the efficiency of both the BE-PL and the Ag^+-PL, in Figure 2c we show the evolution of the respective integrated PL intensity during the scan. For $|V_{EC}|<1.5$ V (patterned area in Figure 2c), no significant effect is observed. This is in agreement with previous SEC results on colloidal nanostructures using ITO/ZnO substrates and is due to the combined effect of the dielectric organic ligands on the NC surfaces and of the potential drop across the ZnO layer that is inserted to suppress PL quenching by energy- or charge-transfer from the NCs to the ITO substrate.[28,83,84] The introduction of the additional ZnO spacer along with the presence of insulating surface ligands can also lead to an appreciable attenuation of the actual shift of the Fermi level compared to the nominal applied EC potential[85]. At negative $V_{EC}\geq -1.5$ V, both PL intensities undergo a sudden drop, reaching ~40% dimming at $V_{EC} = -2.5$ V. For both emissions, when returning back to V_{EC}=0V, the PL intensity progressively increases resulting in nearly complete (~90%) recovery of the original intensity at V_{EC}=0V. We notice that the PL brightening is markedly slower than the respective drop and proceeds over time also when no potential is applied, with an additional 5% recovery after about one minute at V_{EC}=0V (highlighted in grey in Figure 2c). In order to investigate this aspect in deeper detail, we have performed an ON/OFF scan, in which the PL is continuously monitored while the potential, initially set to V_{EC}=0V, is raised to -2.5 V where it is kept constant for 30 s after which it is suddenly brought back to 0V. The evolution of the integrated intensity of both the BE-PL and the Ag^+-PL during the scan are reported in Figure 2d, showing the sudden drop of both bands with applied negative V_{EC} followed by their slow recovery that proceeds over time for about 15 minutes. This indicates that the potential sweep causes no significant damage to the NC surfaces, as confirmed by the inspection of the PL spectra collected for different V_{EC} values (Figure 2e) that show identical emission profiles in all EC conditions. The stability of the NCs to reducing EC potentials is further highlighted in Figure S5 where we report the PL response over four consecutive EC cycles showing reproducible trends with minor progressive dimming due to the incomplete PL recovery over the duration of the measurement. The SEC response is therefore ascribed to reversible

activation/passivation of trap sites likely associated with under-coordinated surface atoms or dangling bonds. Specifically, since the application of negative V_{EC} passivates electron traps and concomitantly activates hole traps, the observed strong drop of the PL intensity suggests that nonradiative trapping of holes in activated defects states is not counterbalanced by the concomitant PL brightening effect of suppressed electron trapping. The slow PL recovery at V_{EC}=0V, in turn, suggests very slow detrapping rate for trapped holes, in agreement with previous results showing very long discharging time in IV-VI NCs.[86] Most importantly, the similar response of the BE-PL and the Ag^+ emission, both in terms of threshold V_{EC}-value and relative amplitude of the intensity drop, indicates that the intrinsic and dopant-related decay pathways are equally quenched by hole trapping, which confirms the picture of the dopant-related emission requiring the localization of a photoexcited VB hole in the Ag^+ site to activate its capability of radiatively accepting a CB electron.

We next performed SEC measurements under positive potentials which provide complementary insight into the nature of the surface defect states. The results, reported in Figure 2g, show no variation of either the BE-PL or the Ag^+-PL for V_{EC} up to 1.5 V. Since these NCs are not passivated with a thick wide energy gap shell that suppresses electron trapping, the absence of a quenching effect by positive V_{EC} points to a situation in which localized states are positioned in energy just above the FL of the NCs, that is, they are already devoid of electrons at V_{EC}=0V, as schematically depicted in Figure 2a. As a result, similar to what recently observed in $CsPbBr_3$ perovskite NCs,[84] their occupancy cannot be further reduced by the application of positive V_{EC}, which makes the PL efficiency essentially insensitive to oxidative potentials. This argument also explains the absence of a PL brightening effect due to suppressed hole trapping by EC removal of excess electrons localized in NC surface states and further indicates that, in unperturbed conditions, electron trapping is the main responsible for the nonradiative losses in our NCs (PL quantum yield, Φ_{PL}~5%). Finally, the position of the localized states deep inside the NC energy gap is in agreement with the observed

minute-long detrapping time of trapped holes after the removal of negative V_{EC} leading to the marked asymmetry between the dimming versus brightening dynamics shown in Figure 2c and 2d.

Magnetic circular dichroism measurements. One important consequence of the recombination mechanism emerging from the PL and TA measurements as well as from the SEC analysis is that the optical activity (that is, the electron-accepting capability) of the dopant site depends on the transient excitation of the Ag^+ ion from its $4d^{10}$ ground state configuration with nonmagnetic character to $4d^9$ with paramagnetic behaviour. An analogous process underpins the optical excitation of Cu^+-doped NCs, leading to the transient formation of paramagnetic Cu^{2+} centres whose unpaired electron spin in the 3*d* state leads to a strong *sp-d* spin-exchange interaction between the 1S exciton and the embedded paramagnetic Cu^{2+}.[29] In Ag-doped NCs, because of the large second ionization energy of Ag not being compensated by the local lattice distortion, such behaviour would be somewhat unexpected. On the other hand, an experimental observation of *sp-d* exchange between the NC bands and any unpaired *d*-electrons of silver, would unambiguously indicate that capture of the VB hole leads to a metastable Ag^{+2}-like excited state in CdSe NCs and would demonstrate that DMS physics can be triggered optically in NCs with nonmagnetic dopants.

In order to address this aspect, we performed MCD experiments as a function of temperature and magnetic field. In Figure 3a, we report the MCD spectra of Ag:CdSe NCs at increasing magnetic field up to B=7 T at 3 K, together with the corresponding linear absorption spectrum. The MCD spectrum shows two main peaks at ~2.15 eV and ~2.6 eV corresponding to the NC's 1S and 2S exciton absorption peaks and a minor contribution at 1.9 eV due to direct absorption by the Ag^+ dopants.

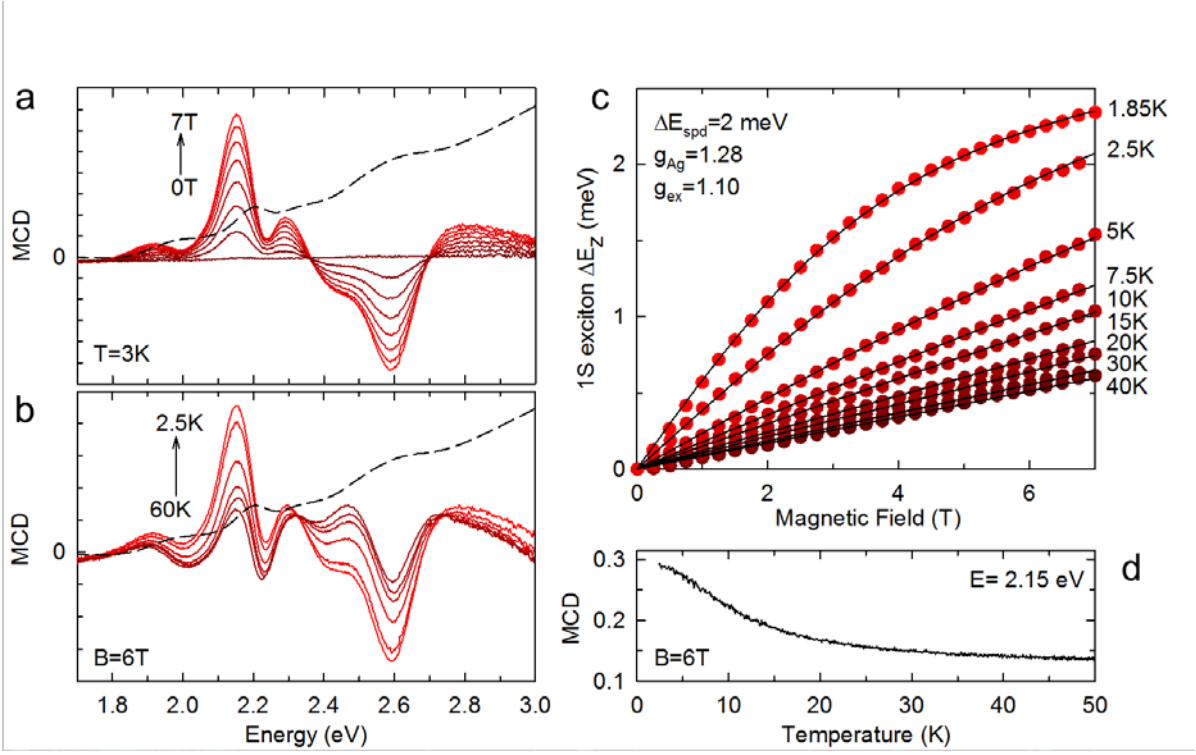

Figure 3. MCD physics in Ag-doped nanocrystals. a, MCD spectra of Ag:CdSe NCs, from which the Zeeman splitting of the 1S exciton can be inferred. MCD spectra are shown at 3 K in different magnetic fields from 0 to 7 T. **b**, MCD spectra at 6 T, at temperatures from 2.5 to 60 K. The linear absorption spectrum is reported as dashed black line in both 'a' and 'b' for direct comparison with the MCD spectrum. **c**, Enhanced Zeeman splitting of the 1S band-edge exciton versus magnetic field, at different temperatures. The high field saturation and strong temperature dependence indicate the existence of *sp–d* exchange coupling between the conduction/valence bands of the semiconductor host and a paramagnetic species in the nanocrystals. This species is likely Ag dopants excited by fast localization (capture) of the valence band hole. Lines are fits to a Brillouin function using a single set of parameters. **d**. Intensity of the MCD signal of the 1S exciton at 6T as a function of temperature from 2.5 K to 50 K.

Fundamentally, the magnetic response of the 1S absorption peak shows intensification with increasing magnetic field and decreasing temperature (Figure 3b), revealing strong paramagnetic response. We stress that, temperature-dependence of the MCD is the most direct and arguably the only definitive indication of the presence of coupling between carriers in the NC bands and paramagnetic species.[29,32,35,87] Data in Figure 4 are therefore unambiguous signatures of *sp-d* exchange due to the progressive alignment of the photoexcited Ag^{2+} spins to the magnetic field. This provides the first demonstration of photoinduced DMS physics in Ag-doped NCs.[88] To further quantify this effect, we extracted the Zeeman splitting energy (ΔE_Z) of the 1S exciton as a function of B and temperature. In Figure 3c, we report the evolution of ΔE_Z upon continuously increasing B

from 0 to 7 T in the 1.85-40 K temperature range. In agreement with Figure 3a and 3b, ΔE_Z is markedly temperature-dependent and shows clear saturation for T<5 K. This is further supported by the fitting of ΔE_Z with the standard Brillouin functional form for conventional DMS materials:[88]

$$\Delta E_Z = g_{ex}\mu_B B + \Delta E_{sp-d} \cdot B_J\left(\frac{g_{Ag}\mu_B JB}{k_B T}\right) \quad (1)$$

where the first term is the linear and temperature-independent Zeeman splitting arising from the intrinsic Landé-factor of the CdSe exciton (g_{ex})[89] and the second term accounts for any additional splitting due to the *sp-d* exchange interaction between the semiconductor bands and the dopant spins.[88] The magnitude of *sp-d* splitting energy, ΔE_{sp-d}, is weighted for the average spin projection along the magnetic field, which is modelled by the Brillouin function $B_J\left(\frac{g_{Ag}\mu_B JB}{k_B T}\right)$, describing the magnetic field and temperature dependent paramagnetism of the ions with spin *J*. Here, g_{Ag} is the Ag^{2+} g-factor, μ_B is the Bohr magneton and k_B the Boltzmann constant. For d^9 dopants in II-VI compounds,[90,91] the tetragonal crystal field lowers and increases the energy of the six-fold degenerate t_{2g}-states and of the four-fold degenerate e_g-states respectively. Therefore, we use *J*=1/2 for the lowest Kramer doublet to fit the experimental data with Eq.(1) (black lines, Figure 3c), setting as shared parameters the *sp-d* exchange interaction and the exciton and dopant Landé-factors. The best fit of whole set of data in Figure 3c is obtained using ΔE_{sp-d}=2.00 meV, g_{ex}=1.10, and g_{Ag}=1.28. The obtained g_{ex} is comparable to the values reported for both undoped[89,92] and copper-doped CdSe NCs[87], and g_{Ag} is consistent to Ag-doped bulk ZnSe showing magnetic response that was suggested to originate from a photoexcited $[Ag_{Zn}^{2+}\text{-}Se^{2-}\text{-}Ag_i^{+}]^{+}$ paramagnetic acceptor complex involving a substitutional and an interstitial silver ion.[93] The effect of temperature on the MCD intensity at the 1S absorption energy is quantified in Figure 3d, confirming the strong paramagnetic response below T=20K.

Photoinduced paramagnetism in Ag:CdSe NCs. We highlight that the observed magnetic behaviour in Ag:CdSe NCs is not a ground-state property, but a photoinduced effect due to the probe light that

is used for the MCD measurements that necessarily matches the absorption spectrum of the NCs. This effect is highlighted in Figure 4a, showing progressively stronger MCD signal with increasing probe intensity. This behaviour is unusual because the MCD signal is an intrinsically normalized physical quantity corresponding to the ratio between the absorption difference of right- and left-circularly polarized light and the intensity of the transmitted portion of the light probe. Therefore, the amplitude of the MCD signal for conventional magnetic materials is independent of the intensity of the probe beam. Conversely, in our case the observed strong dependence of the MCD amplitude on the probe intensity is direct consequence of the particular physics of Ag^{+} dopants in CdSe NCs. To further investigate this aspect, we performed MCD spectroscopy at B=6 T in the presence and in the absence of additional 3.05 eV laser excitation (excitation fluence ~10μW/mm^2). In order to avoid parasitic heating effects, we performed the experiments in superfluid helium at T=1.8K, which ensures optimal heat sinking. Remarkably, as shown in Figure 4b, the MCD signal increases substantially up to by ~100% upon additional illumination with UV light without any spectral modification. The effect of the additional illumination is further emphasized in Figure 4c, where we report the MCD signal of the 1S absorption peak at 2.15 eV during a magnetic field ramp up to 7T, with and without additional UV illumination, confirming, in both cases, the strongly nonlinear field-dependence characteristic of *sp-d* exchange (Figure 3c). Apart from the low-field region (<2 T), both trends are well described by Eq.(1) using appropriate scaling of $\Delta E_{sp\text{-}d}$ to account for the larger number of photo-activated paramagnetic impurities in the sample.

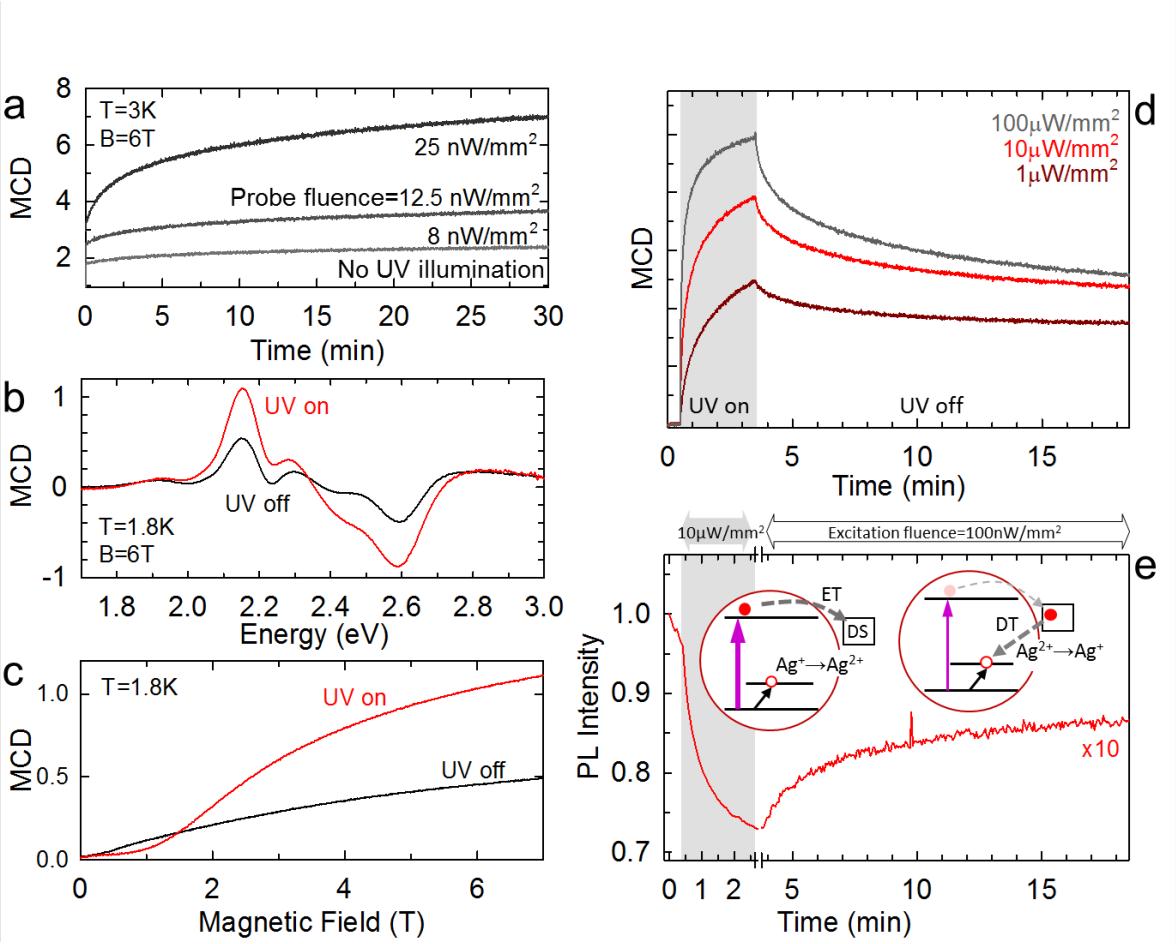

Figure.4 Photoinduced paramagnetization of Ag-doped CdSe nanocrystals. a, Evolution of the MCD signal of the 1S exciton of Ag:CdSe NCs over time measured at 3K and 6T using increasingly higher probe fluence. **b**, MCD signals measured at constant probe intensity in the presence (red line) and in the absence (black line) of additional illumination with 3.1 eV ultraviolet light (100 μW/mm^2). **c**, Peak MCD signal (measured at 2.15 eV) as a continuous function of applied magnetic field with and without additional UV illumination (100 μW/mm^2). **d**, Time evolution of the peak MCD signal as the additional UV illumination is turned on (grey shading) and off. Stronger UV light leads to larger MCD signal and faster dynamics of both 'on' and 'off' phases. In all cases, the MCD decay is markedly slower than the corresponding rise under UV excitation. **e**, Time evolution of the integrated PL intensity under low or high excitation regimes, corresponding to the UV-off and UV-on conditions in the MCD scan in 'd'. The time axes are on the same scale for direct comparison of the similar temporal dynamics, emphasizing the close anti-correlation between the PL intensity and MCD signal. Inset: schematic depiction of the electron trapping(ET)/detrapping(DT) mechanisms in defect states (DS) responsible for the ultra-long lifetime of the metastable paramagnetic state. Under intense (10μW/mm^2) UV excitation (left scheme), the PL is quenched by ET that enhances the MCD signal in 'd' by favouring the accumulation of photoinduced paramagnetic Ag^{2+} states. When the UV excitation is lowered to 100nW/mm^2 (right scheme), slow DT of trapped electrons leads to recovery of the PL signal and concomitant decrease of the MCD intensity.

To gather deeper insights into the effect of photoexcitation on the magnetic response of Ag:CdSe NCs and to identify correlations with the exciton recombination mechanism emerging from the SEC results, we monitored the evolution of the photoinduced MCD over time as a function of the UV

excitation fluence. As shown in Figure 4d, increasing the fluence of the UV light leads to faster MCD growth and higher maximum values (as measured after 3 minutes monitoring), confirming the direct relationship between the magnetization and NC excitation. Interestingly, for all fluence used, when the UV laser is turned off, the MCD signal decreases very slowly over several minutes. Such minute-long persistence of the metastable paramagnetic state, extending for over nine orders of magnitude longer than the dopant emission lifetime (~220 ns, Figure 1b), indicates that radiative capture of the CB electron in the silver state is not the determining process in the $Ag^{2+} \rightarrow Ag^{+}$ dynamics responsible for the drop of the photoinduced MCD. This effect can be explained by the presence of localized states positioned in energy above the NC Fermi energy efficiently trapping CB electrons, as indicated by SEC in Figure 2. As a result of electron trapping, the lifetime of the metastable paramagnetic state would be dramatically extended with respect to the corresponding PL decay and the MCD recovery time would be dictated by the electron detrapping dynamics (see scheme in Figure 4d). This suggests a direct correlation between the MCD growth (drop) and the PL dimming (brightening) due to carrier trapping (detrapping). In order to experimentally validate this hypothesis, we monitored the PL intensity of the Ag-doped NCs film over an analogous time scale as the MCD time trace. To reproduce the conditions of the MCD scan in the absence of additional UV illumination, we used 3.1 eV light with 100 nW/mm^2 fluence. The situation in which the sample is exposed to further UV excitation is recreated by increasing the fluence to 10μW/mm^2, corresponding to the laser intensity used in the photoinduced MCD experiments. We stress that, in all excitation conditions, the excitation rate is well below 10^{-3} excitons/NC, thus excluding multiexcitonic effects. Figure 4e shows the remarkable anti-correlation between the PL trend and the MCD time trace in Figure 4d, with the emission intensity undergoing a relatively faster drop under intense UV excitation due to progressive photocharging by electron trapping, while the MCD signal is concomitantly strongly intensified. Once the excitation fluence is reduced to 100 nW/mm^2, the PL intensity is slowly recovered on a time scale compatible to the slow decay of the photoinduced MCD. This result confirms the above

assumption that the process responsible for the persistence of the photoinduced magnetism is likely the slow release of CB electrons trapped in relatively deep acceptor surface states.

In summary, through the combination of complementary optical, spectroelectrochemical and magnetic circular dichroism experiments we showed that nanocrystals doped with silver ions exhibit optically-activated paramagnetic properties and concomitant *sp–d* exchange interactions between excitons and Ag dopants, suggesting that optically switchable magnetic nanomaterials can be obtained by exploiting the excitonic processes involving nominally nonmagnetic impurities.

Methods

Synthesis of Ag-doped CdSe NCs.

Sythesis of 3% Ag doped CdSe QDs(~5 nm)**:** CdSe QDs were synthesized via the in-situ sulfuration and cation exchange reaction of the Ag NPs. In this work, monodisperse Ag NPs (~5 nm) were prepared first according to Li et al.,[78] which can be further used in the preparation of amorphous Ag_2Se NPs by the sulfuration with a Se precursor in the molar ratio of 1:5 at 50 ℃.The Se precursor was prepared from 1 mmol Se powder with 7 mL octadecylene at 270 °C. The obtained Ag_2Se NCs (0.035 mmol) were dispersed in 10 mL toluene with 0.2 mL OA and 0.1 mL OAm. After that, 1 ml methanol solution containing 0.1 g of $Cd(NO_3)_2 \cdot 4H_2O$ was added. After 2 min magnetic stirring, 0.1 mL TBP was added, and the mixture was heated at 55 °C for 1 h under magnetic stirring.

Structural Characterization.

Samples for TEM characterization were prepared by placing one drop of toluene solution, together with the product, onto a 300 mesh copper grid with a carbon support fi lm. A JEOL JEM 1200EX working at 100 kV and a HRTEM (FEI Tecnai G2 F20 S-Twin working at 200 kV) were utilized to characterize the morphology of CdSe QDs.

The XPS spectra were obtained with a PHI Quantera II X-ray photoelectron spectrometer using Al Kα non-monochromatic radiation. The colloidal NPs were dip-coated on silicon substrate for XPS characterization. The measurement parameters were: light spot size 100 μm; power 100 W; voltage 20 kV. An energy correction was made to account for sample charging based on the C1s peak at 284.8 eV. The elemental concentrations were reported relative to carbon, calculated from the XPS spectra based on the area of the characteristic photoelectron peaks after correcting for atomic sensitivity.

Spectroscopic Studies. The absorption spectra were recorded using a Varian Cary 50 spectrophotometer. The PL measurements were performed using a pulsed diode laser at 3.1 eV (Edinburg Inst. EPL 405, 40 ps pulse width) as excitation source and collecting the emitted light with a TM-C10083CA Hamamatsu Mini-Spectrometer. Time-resolved photoluminescence experiments were conducted using the same excitation source and collecting with a Hamamtsu R943-02 time-correlated single photon counting unit coupled to an Oriel Instrument Cornerstone 260 monochromator. All PL measurements were performed with power density of 100 nJ/cm^2. For PLE and PL experiments under resonant excitation conditions, a spectrally narrow photoexcitation source (<0.5nm full width at half maximum) was produced by filtering the output of a 150 W Xenon lamp with a 1/3 m double-grating Gemini monochromator. The emitted PL was collected with a Horiba Scientific Triax 180 1/2 m spectrograph and detected with an Instrument SA Spectrum One liquid-nitrogen-cooled charge-coupled device (CCD). All measurements were carried out at room temperature except the photocharging experiments that were conducted at 18 K.

Transient transmission spectroscopy.

For the ultrafast transient transmission measurements, the laser source was a Ti:sapphire laser with chirped pulse amplification (Coherent LIBRA-HE), which provided 95 fs pulses at 800 nm at a repetition rate of 2 kHz. The excitation pulses at 2.3eV (540nm) and 2eV (630nm) were generated with an Optical Parametric Amplifier (OPA). The bandwith of the pump pulses is 10nm which correspond to a pulse duration ~100fs. The probe beam was a white light supercontinuum generated by focusing a small fraction of the fundamental beam onto a 2mm thick sapphire plate. The supercontinuum spectrum extends from 450 nm to 1.6 μm, with a gap only around the fundamental wavelength at 800 nm. Pump and probe are then focused on the sample by means of a lens and a spherical mirror. Pump fluences in the position of the white light focus are in the order of $35 \mu Jcm^{-2}$ and 95 μJcm^{-2} for 2.3eV and 2eV pump respectively.

A computer-controlled optical multichannel analyzer working at 1kHz acquires the map of the differential transmission $\Delta T/T = (T_{on} - T_{off})/T_{off}$, as a function of the pump−probe time delay; T_{on} and T_{off} are the probe spectra transmitted by the excited and unperturbed samples.

Spectro-electrochemical Measurements. Indium tin oxide (ITO) coated glass slides (50×7×0.7 mm, R_S < 100Ω) were purchased from Delta Technologies (Part No. CG-90IN-CUV). The ITO coated surface was first covered with zinc oxide (ZnO) nanoparticles (NP) (Nanograde, ~50 nm diameter) to avoid quenching of NC emission by fast charge/energy-transfer to ITO. The ZnO NP layer (~60 nm thick, as measured using a Dektak profilometer) was deposited by dip-coating the glass/ITO substrate into an ethanol suspension of ZnO NPs (2 mg/mL, one dip for 10 s) and annealed at 150° C for 10 min in a nitrogen glovebox. To test the stability of the glass/ITO/ZnO NP substrates during the potential scans, we performed control experiments in which we monitored changes in optical absorption spectra for prolonged exposures to negative and positive potentials. The results of these measurements indicate that the substrates are unaffected by either positive or negative EC potentials for exposure times of tens of minutes, which are much longer than the measurement time used in our SEC experiments (~10 min). The NCs were deposited onto the ZnO NP layer as a few-monolayer-thick film by dip-coating from a dilute toluene solution (optical density of 0.07 at 500 nm; 2 dips for 10 s). The ZnO NPs layer used in this study was not treated with cross-linkers as in [*J. Phys. Chem. C* **2010,** 114, (49), 21138-21141] and therefore it represented a dielectric tunneling barrier of ~1 V. The ITO was connected as a working electrode to the potentiostat (Bio Logic SP-200 Research grade Potentiostat/Galvanostat) and the film was placed into a quartz cuvette filled with the electrolyte (0.1 M tetrabutylammonium perchlorate ($TBAClO_4$) in propylene carbonate). Silver and platinum wires were used as quasi-reference and counter electrodes, respectively. All potentials reported in this work are measured relative to the quasi-reference silver electrode during staircase voltammetry scans (10 s scan rate). The film was excited at 3.1 eV with continuous wave diode lasers and the emitted light was collected with a focusing lens and sent to a spectrometer coupled to a USB4000 OceanOptics spectrometer.

MCD Measurements. MCD measures the normalized difference in transmission between left- and right- circularly polarized light through films of nanocrystals in the Faraday geometry[35]. Nanocrystal films were mounted in the variable-temperature insert (1.5–300 K) of a 7 T superconducting magnet with direct optical access. Probe light of tunable wavelength was derived from a Xenon lamp directed through a spectrometer. The probe light was mechanically chopped at 137 Hz, and was modulated between right and left circular polarizations at 50 kHz using a photoelastic modulator. The transmitted light was detected with a silicon avalanche photodiode. Photomagnetization was induced with additional light from a continuous wave 3.1 eV diode laser.

References

1 Pietryga, J. M., Park, Y.-S., Lim, J., Fidler, A. F., Bae, W. K., Brovelli, S. & Klimov, V. I. Spectroscopic and Device Aspects of Nanocrystal Quantum Dots. *Chemical Reviews* **116**, 10513-10622 (2016).

2 Kovalenko, M. V., Manna, L., Cabot, A., Hens, Z., Talapin, D. V., Kagan, C. R., Klimov, V. I., Rogach, A. L., Reiss, P., Milliron, D. J., Guyot-Sionnnest, P., Konstantatos, G., Parak, W. J., Hyeon, T., Korgel, B. A., Murray, C. B. & Heiss, W. Prospects of Nanoscience with Nanocrystals. *ACS Nano* **9**, 1012-1057 (2015).

3 Bae, W. K., Brovelli, S. & Klimov, V. I. Spectroscopic Insights into the Performance of Quantum Dot Light Emitting Diodes. *Mrs Bulletin* **38**, 721-730 (2013).

4 Dai, X., Zhang, Z., Jin, Y., Niu, Y., Cao, H., Liang, X., Chen, L., Wang, J. & Peng, X. Solution-processed, high-performance light-emitting diodes based on quantum dots. *Nature* **515**, 96-99 (2014).

5 Dang, C., Lee, J., Breen, C., Steckel, J. S., Coe-Sullivan, S. & Nurmikko, A. Red, green and blue lasing enabled by single-exciton gain in colloidal quantum dot films. *Nat Nano* **7**, 335-339 (2012).

6 Sargent, E. H. Colloidal quantum dot solar cells. *Nat Photon* **6**, 133-135 (2012).

7 García de Arquer, F. P., Armin, A., Meredith, P. & Sargent, E. H. Solution-processed semiconductors for next-generation photodetectors. **2**, 16100 (2017).

8 Lorenzon, M., Pinchetti, V., Bruni, F., Bae, W. K., Meinardi, F., Klimov, V. I. & Brovelli, S. Single-Particle Ratiometric Pressure Sensing Based on “Double-Sensor” Colloidal Nanocrystals. *Nano Letters* **17**, 1071-1081 (2017).

9 Medintz, I. L., Uyeda, H. T., Goldman, E. R. & Mattoussi, H. Quantum dot bioconjugates for imaging, labelling and sensing. *Nat Mater* **4**, 435-446 (2005).

10 Bruni, F., Pedrini, J., Bossio, C., Santiago-Gonzalez, B., Meinardi, F., Bae, W. K., Klimov, V. I., Lanzani, G. & Brovelli, S. Two-color emitting colloidal nanocrystals as single particle ratiometric probes of intracellular pH. *Advanced Functional Materials* **Early view** (2016).

11 Meinardi, F., Ehrenberg, S., Dhamo, L., Carulli, F., Mauri, M., Bruni, F., Simonutti, R., Kortshagen, U. & Brovelli, S. Highly efficient luminescent solar concentrators based on earth-abundant indirect-bandgap silicon quantum dots. *Nature Photonics* **11**, 177-185 (2017).

12 Meinardi, F., McDaniel, H., Carulli, F., Colombo, A., Velizhanin, K. A., Makarov, N. S., Simonutti, R., Klimov, V. I. & Brovelli, S. Highly efficient large-area colourless luminescent solar concentrators using heavy-metal-free colloidal quantum dots. *Nat. Nanotechnol.* **10**, 878-885 (2015).

13 Meinardi, F., Colombo, A., Velizhanin, K. A., Simonutti, R., Lorenzon, M., Beverina, L., Viswanatha, R., Klimov, V. I. & Brovelli, S. Large-area luminescent solar concentrators based on /`Stokes-shift-engineered/' nanocrystals in a mass-polymerized PMMA matrix. *Nat Photon* **8**, 392-399 (2014).

14 Bradshaw, L. R., Knowles, K. E., McDowall, S. & Gamelin, D. R. Nanocrystals for luminescent solar concentrators. *Nano Lett* **15**, 1315-1323 (2015).

15 Sharma, M., Gungor, K., Yeltik, A., Olutas, M., Guzelturk, B., Kelestemur, Y., Erdem, T., Delikanli, S., McBride, J. R. & Demir, H. V. Near-Unity Emitting Copper-Doped Colloidal Semiconductor Quantum Wells for Luminescent Solar Concentrators. *Adv Mater* (2017).

16 Zhou, Y., Benetti, D., Fan, Z., Zhao, H., Ma, D., Govorov, A. O., Vomiero, A. & Rosei, F. Near Infrared, Highly Efficient Luminescent Solar Concentrators. *Advanced Energy Materials* **6**, 1501913 (2016).

17 Rossetti, R., Ellison, J., Gibson, J. & Brus, L. Size effects in the excited electronic states of small colloidal CdS crystallites. *The Journal of Chemical Physics* **80**, 4464-4469 (1984).

18 Brus, L. E. A simple model for the ionization potential, electron affinity, and aqueous redox potentials of small semiconductor crystallites. *The Journal of Chemical Physics* **79**, 5566-5571 (1983).
19 Donega, C. d. M. Synthesis and properties of colloidal heteronanocrystals. *Chemical Society Reviews* **40**, 1512-1546 (2011).
20 Brovelli, S., Schaller, R. D., Crooker, S. A., García-Santamaría, F., Chen, Y., Viswanatha, R., Hollingsworth, J. A., Htoon, H. & Klimov, V. I. Nano-engineered electron-hole exchange interaction controls exciton dynamics in core-shell semiconductor nanocrystals. *Nature Communications* **2** (2011).
21 Christodoulou, S., Rajadell, F., Casu, A., Vaccaro, G., Grim, J., Genovese, A., Manna, L., Climente, J. I., Meinardi, F., Rainò, G., Stöferle, T., Mahrt, R. F., Planelles, J., Brovelli, S. & Moreels, I. Band Structure Engineering via Piezo-Electric Fields in Strained Anisotropic CdSe/CdS Nanocrystals. *Nature Communications* **6**, 7905 (2015).
22 Norris, D. J., Efros, A. L. & Erwin, S. C. Doped nanocrystals. *Science* **319**, 1776-1779 (2008).
23 Erwin, S. C., Zu, L. J., Haftel, M. I., Efros, A. L., Kennedy, T. A. & Norris, D. J. Doping semiconductor nanocrystals. *Nature* **436**, 91-94 (2005).
24 Erwin, S. C., Zu, L., Haftel, M. I., Efros, A. L., Kennedy, T. A. & Norris, D. J. Doping semiconductor nanocrystals. *Nature* **436**, 91-94 (2005).
25 Norris, D. J., Yao, N., Charnock, F. T. & Kennedy, T. A. High-Quality Manganese-Doped ZnSe Nanocrystals. *Nano Letters* **1**, 3-7 (2001).
26 Sapra, S., Prakash, A., Ghangrekar, A., Periasamy, N. & Sarma, D. D. Emission Properties of Manganese-Doped ZnS Nanocrystals. *The Journal of Physical Chemistry B* **109**, 1663-1668 (2005).
27 Bhargava, R. N., Gallagher, D., Hong, X. & Nurmikko, A. Optical properties of manganese-doped nanocrystals of ZnS. *Physical Review Letters* **72**, 416-419 (1994).
28 Brovelli, S., Galland, C., Viswanatha, R. & Klimov, V. I. Tuning Radiative Recombination in Cu-Doped Nanocrystals via Electrochemical Control of Surface Trapping. *Nano Letters* **12**, 4372-4379 (2012).
29 Pandey, A., Brovelli, S., Viswanatha, R., Li, L., Pietryga, J. M., Klimov, V. I. & Crooker, S. A. Long-lived photoinduced magnetization in copper-doped ZnSe-CdSe core-shell nanocrystals. *Nat Nano* **7**, 792-797 (2012).
30 Jana, S., Manna, G., Srivastava, B. B. & Pradhan, N. Tuning the emission colors of semiconductor nanocrystals beyond their bandgap tunability: all in the dope. *Small* **9**, 3753-3758 (2013).
31 Srivastava, B. B., Jana, S. & Pradhan, N. Doping Cu in Semiconductor Nanocrystals: Some Old and Some New Physical Insights. *Journal of the American Chemical Society* **133**, 1007-1015 (2010).
32 Yu, J. H., Liu, X., Kweon, K. E., Joo, J., Park, J., Ko, K. T., Lee, D. W., Shen, S., Tivakornsasithorn, K., Son, J. S., Park, J. H., Kim, Y. W., Hwang, G. S., Dobrowolska, M., Furdyna, J. K. & Hyeon, T. Giant Zeeman splitting in nucleation-controlled doped CdSe:Mn2+ quantum nanoribbons. *Nat Mater* **9**, 47-53 (2010).
33 Sahu, A., Kang, M. S., Kompch, A., Notthoff, C., Wills, A. W., Deng, D., Winterer, M., Frisbie, C. D. & Norris, D. J. Electronic Impurity Doping in CdSe Nanocrystals. *Nano Letters* **12**, 2587-2594 (2012).
34 Kang, M. S., Sahu, A., Frisbie, C. D. & Norris, D. J. Influence of Silver Doping on Electron Transport in Thin Films of PbSe Nanocrystals. *Advanced Materials* **25**, 725-731 (2013).
35 Bussian, D. A., Crooker, S. A., Yin, M., Brynda, M., Efros, A. L. & Klimov, V. I. Tunable magnetic exchange interactions in manganese-doped inverted core-shell ZnSe-CdSe nanocrystals. *Nat Mater* **8**, 35-40 (2009).

36 Merkulov, I. A., Yakovlev, D. R., Keller, A., Ossau, W., Geurts, J., Waag, A., Landwehr, G., Karczewski, G., Wojtowicz, T. & Kossut, J. Kinetic Exchange between the Conduction Band Electrons and Magnetic Ions in Quantum-Confined Structures. *Physical Review Letters* **83**, 1431-1434 (1999).
37 Ochsenbein, S. T., Feng, Y., Whitaker, K. M., Badaeva, E., Liu, W. K., Li, X. & Gamelin, D. R. Charge-controlled magnetism in colloidal doped semiconductor nanocrystals. *Nat Nano* **4**, 681-687 (2009).
38 Norris, D. J., Yao, N., Charnock, F. T. & Kennedy, T. A. High-quality manganese-doped ZnSe nanocrystals. *Nano Letters* **1**, 3-7 (2001).
39 Bussian, D. A., Crooker, S. A., Yin, M., Brynda, M., Efros, A. L. & Klimov, V. I. Tunable magnetic exchange interactions in manganese-doped inverted core–shell ZnSe–CdSe nanocrystals. *Nature Materials* **8**, 35-40 (2008).
40 Beaulac, R., Feng, Y., May, J. W., Badaeva, E., Gamelin, D. R. & Li, X. Orbital pathways for Mn2+-carrier sp-d exchange in diluted magnetic semiconductor quantum dots. *Physical Review B - Condensed Matter and Materials Physics* **84** (2011).
41 Fainblat, R., Barrows, C. J., Hopmann, E., Siebeneicher, S., Vlaskin, V. A., Gamelin, D. R. & Bacher, G. Giant Excitonic Exchange Splittings at Zero Field in Single Colloidal CdSe Quantum Dots Doped with Individual Mn2+ Impurities. *Nano Lett* (2016).
42 Nag, A., Chakraborty, S. & Sarma, D. D. To dope Mn^{2+} in a semiconducting nanocrystal. *Journal of the American Chemical Society* **130**, 10605-10611 (2008).
43 Rice, W. D., Liu, W., Pinchetti, V., Yakovlev, D. R., Klimov, V. I. & Crooker, S. A. Direct Measurements of Magnetic Polarons in Cd1–xMnxSe Nanocrystals from Resonant Photoluminescence. *Nano Letters* (2017).
44 Beaulac, R., Schneider, L., Archer, P. I., Bacher, G. & Gamelin, D. R. Light-Induced Spontaneous Magnetization in Doped Colloidal Quantum Dots. *Science* **325**, 973-976 (2009).
45 Rice, W. D., Liu, W., Pinchetti, V., Yakovlev, D. R., Klimov, V. I. & Crooker, S. A. Direct Measurements of Magnetic Polarons in Cd1-xMnxSe Nanocrystals from Resonant Photoluminescence. *Nano Lett* **17**, 3068-3075 (2017).
46 Muckel, F., Barrows, C. J., Graf, A., Schmitz, A., Erickson, C. S., Gamelin, D. R. & Bacher, G. Current-induced magnetic polarons in a colloidal quantum-dot device. *Nano Lett* (2017).
47 Krustok, J., Mädasson, J., Altosaar, M. & Kukk, P. The nature of recombination centres in silver- and chlorine-doped CdS phosphors. *Journal of Physics and Chemistry of Solids* **51**, 1013-1018 (1990).
48 Krustok, J. Orange luminescence of donor-acceptor pairs in CdS:Ag:Cl. *Journal of Physics and Chemistry of Solids* **53**, 1027-1030 (1992).
49 Peka, P. & Schulz, H. J. Empirical one-electron model of optical-transitions in Cu-doped ZnS and CdS. *Physica B* **193**, 57-65 (1994).
50 Stringfellow G. B. & Bube, R. H. Photoelectronic Properties of ZnSe Crystals. *Physical Review* **171**, 903–915 (1968).
51 Srivastava, B. B., Jana, S. & Pradhan, N. Doping Cu in Semiconductor Nanocrystals: Some Old and Some New Physical Insights. *Journal of the American Chemical Society* **133**, 1007-1015 (2011).
52 Viswanatha, R., Brovelli, S., Pandey, A., Crooker, S. A. & Klimov, V. I. Copper-Doped Inverted Core/Shell Nanocrystals with “Permanent” Optically Active Holes. *Nano Letters* **11**, 4753-4758 (2011).
53 Nelson, H. D., Hinterding, S. O. M., Fainblat, R., Creutz, S. E., Li, X. & Gamelin, D. R. Mid-Gap States and Normal vs Inverted Bonding in Luminescent Cu+- and Ag+-Doped CdSe Nanocrystals. *J Am Chem Soc* **139**, 6411-6421 (2017).

54 Grandhi, G. K., Tomar, R. & Viswanatha, R. Study of surface and bulk electronic structure of II-VI semiconductor nanocrystals using Cu as a nanosensor. *ACS Nano* **6**, 9751-9763 (2012).
55 Grandhi, G. K. & Viswanatha, R. Tunable infrared phosphors using Cu doping in semiconductor nanocrystals: Surface electronic structure evaluation. *Journal of Physical Chemistry Letters* **4**, 409-415 (2013).
56 Liu, J., Zhao, Q., Liu, J.-L., Wu, Y.-S., Cheng, Y., Ji, M.-W., Qian, H.-M., Hao, W.-C., Zhang, L.-J., Wei, X.-J., Wang, S.-G., Zhang, J.-T., Du, Y., Dou, S.-X. & Zhu, H.-S. Heterovalent-Doping-Enabled Efficient Dopant Luminescence and Controllable Electronic Impurity Via a New Strategy of Preparing II−VI Nanocrystals. *Advanced Materials* **27**, 2753-2761 (2015).
57 Santiago-González, B., Monguzzi, A., Pinchetti, V., Casu, A., Prato, M., Lorenzi, R., Campione, M., Chiodini, N., Santambrogio, C., Meinardi, F., Manna, L. & Brovelli, S. "Quantized" Doping of Individual Colloidal Nanocrystals Using Size-Focused Metal Quantum Clusters. *ACS Nano* (2017).
58 Mocatta, D., Cohen, G., Schattner, J., Millo, O., Rabani, E. & Banin, U. Heavily Doped Semiconductor Nanocrystal Quantum Dots. *Science* **332**, 77-81 (2011).
59 Ding, S.-J., Nan, F., Liu, X.-N., Liu, X.-L., Zhang, Y.-F., Liang, S., Yao, D.-Z., Zhang, X.-H. & Wang, Q.-Q. Largely Enhanced Optical Nonlinear Response of Heavily Doped Ag:CdTe Nanocrystals around the Excitonic Band Edge. *The Journal of Physical Chemistry C* **119**, 24958-24964 (2015).
60 Almeida, A. J., Sahu, A., Riedinger, A., Norris, D. J., Brandt, M. S., Stutzmann, M. & Pereira, R. N. Charge Trapping Defects in CdSe Nanocrystal Quantum Dots. *The Journal of Physical Chemistry C* **120**, 13763-13770 (2016).
61 Kompch, A., Sahu, A., Notthoff, C., Ott, F., Norris, D. J. & Winterer, M. Localization of Ag Dopant Atoms in CdSe Nanocrystals by Reverse Monte Carlo Analysis of EXAFS Spectra. *The Journal of Physical Chemistry C* **119**, 18762-18772 (2015).
62 Ott, F. D., Spiegel, L. L., Norris, D. J. & Erwin, S. C. Microscopic Theory of Cation Exchange in CdSe Nanocrystals. *Physical Review Letters* **113**, 156803 (2014).
63 Slater, J. C. Atomic Radii in Crystals. *The Journal of Chemical Physics* **41**, 3199-3204 (1964).
64 Grochala, W. & Hoffmann, R. Real and Hypothetical Intermediate-Valence AgII/AgIII and AgII/AgI Fluoride Systems as Potential Superconductors. *Angewandte Chemie International Edition* **40**, 2742-2781 (2001).
65 Broser, I. & Schulz, H. J. A Comparative Study of Infrared Luminescence and some other Optical and Electrical Properties of Zn-Cu Single Crystals. *Journal of The Electrochemical Society* **108**, 545-548 (1961).
66 Grochala, W. & Mazej, Z. Chemistry of silver(II): a cornucopia of peculiaritiesdagger. *Philos Trans A Math Phys Eng Sci* **373** (2015).
67 Dean, P. J., Fitzpatrick, B. J. & Bhargava, R. N. Optical properties of ZnSe doped with Ag and Au. *Physical Review B* **26**, 2016-2035 (1982).
68 Holtz, P. O., Monemar, B. & Loykowski, H. J. Optical properties of Ag-related centers in bulk ZnSe. *Physical Review B* **32**, 986-996 (1985).
69 Nedeoglo, N. D., Sirkeli, V. P., Nedeoglo, D. D., Laiho, R. & Lähderanta, E. Electron configuration and charge state of electrically active Cu, Ag and Au ions in ZnSe. *Journal of Physics: Condensed Matter* **18**, 8113 (2006).
70 McMillan, J. A. Higher Oxidation States of Silver. *Chemical Reviews* **62**, 65-80 (1962).
71 Mazej, Z., Michalowski, T., Goreshnik, E. A., Jaglicic, Z., Arcon, I., Szydlowska, J. & Grochala, W. The first example of a mixed valence ternary compound of silver with random distribution of Ag(I) and Ag(II) cations. *Dalton Trans* **44**, 10957-10968 (2015).

72 Derzsi, M., Dymkowski, K. & Grochala, W. The theoretical quest for sulfate of Ag(2+): genuine Ag(II)SO4, diamagnetic Ag(I)2S2O8, or rather mixed-valence Ag(I)[Ag(III)(SO4)2]? *Inorg Chem* **49**, 2735-2742 (2010).
73 Müller-Rösing, H.-C., Schulz, A. & Hargittai, M. Structure and Bonding in Silver Halides. A Quantum Chemical Study of the Monomers: Ag2X, AgX, AgX2, and AgX3 (X = F, Cl, Br, I). *Journal of the American Chemical Society* **127**, 8133-8145 (2005).
74 Burdett, J. K. & Eisenstein, O. From three- to four-coordination in copper(I) and silver(I). *Inorg Chem* **31**, 1758-1762 (1992).
75 Vydyanath, H. R. & Kröger, F. A. The defect structure of silver-doped CdS. *Journal of Physics and Chemistry of Solids* **36**, 509-520 (1975).
76 Swaminathan, V. & Greene, L. C. Low temperature photoluminescence in Ag-doped ZnSe. *Journal of Luminescence* **14**, 357-363 (1976).
77 Ishizumi, A. & Kanemitsu, Y. Photoluminescence Spectra and Dynamics of Al3+- and Ag+-Doped CdS Nanocrystals. *Journal of the Physical Society of Japan* **79**, 093706 (2010).
78 Li, L., Hu, F., Xu, D., Shen, S. & Wang, Q. Metal ion redox potential plays an important role in high-yield synthesis of monodisperse silver nanoparticles. *Chemical Communications* **48**, 4728-4730 (2012).
79 Yang, L., Knowles, K. E., Gopalan, A., Hughes, K. E., James, M. C. & Gamelin, D. R. One-Pot Synthesis of Monodisperse Colloidal Copper-Doped CdSe Nanocrystals Mediated by Ligand–Copper Interactions. *Chemistry of Materials* **28**, 7375-7384 (2016).
80 Lupo, M. G., Della Sala, F., Carbone, L., Zavelani-Rossi, M., Fiore, A., Lüer, L., Polli, D., Cingolani, R., Manna, L. & Lanzani, G. Ultrafast Electron−Hole Dynamics in Core/Shell CdSe/CdS Dot/Rod Nanocrystals. *Nano Letters* **8**, 4582-4587 (2008).
81 Jha, P. P. & Guyot-Sionnest, P. Trion Decay in Colloidal Quantum Dots. *ACS Nano* **3**, 1011-1015 (2009).
82 Brovelli, S., Bae, W. K., Meinardi, F., Santiago González, B., Lorenzon, M., Galland, C. & Klimov, V. I. Electrochemical Control of Two-Color Emission from Colloidal Dot-in-Bulk Nanocrystals. *Nano Letters* **14**, 3855-3863 (2014).
83 Lorenzon, M., Christodoulou, S., Vaccaro, G., Pedrini, J., Meinardi, F., Moreels, I. & Brovelli, S. Reversed oxygen sensing using colloidal quantum wells towards highly emissive photoresponsive varnishes. *Nat Commun* **6** (2015).
84 Lorenzon, M., Sortino, L., Akkerman, Q., Accornero, S., Pedrini, J., Prato, M., Pinchetti, V., Meinardi, F., Manna, L. & Brovelli, S. Role of Nonradiative Defects and Environmental Oxygen on Exciton Recombination Processes in CsPbBr3 Perovskite Nanocrystals. *Nano Letters* (2017).
85 Dewald, J. F. The charge distribution at the zinc oxide-electrolyte interface. *Journal of Physics and Chemistry of Solids* **14**, 155-161 (1960).
86 Padilha, L. A., Robel, I., Lee, D. C., Nagpal, P., Pietryga, J. M. & Klimov, V. I. Spectral dependence of nanocrystal photoionization probability: the role of hot-carrier transfer. *ACS Nano* **5**, 5045-5055 (2011).
87 Archer, P. I., Santangelo, S. A. & Gamelin, D. R. Direct Observation of sp−d Exchange Interactions in Colloidal Mn2+- and Co2+-Doped CdSe Quantum Dots. *Nano Letters* **7**, 1037-1043 (2007).
88 Furdyna, J. K. Diluted magnetic semiconductors. *Journal of Applied Physics* **64**, R29-R64 (1988).
89 Kuno, M., Nirmal, M., Bawendi, M. G., Efros, A. & Rosen, M. Magnetic circular dichroism study of CdSe quantum dots. *The Journal of Chemical Physics* **108**, 4242-4247 (1998).
90 Schulz, H. J. Optical properties of 3d transition metals in II–VI compounds. *Journal of Crystal Growth* **59**, 65-80 (1982).
91 Schulz, H. J. Transition metal impurities in compound semiconductors: Experimental situation. *Materials Chemistry and Physics* **16**, 373-384 (1987).

92 Gupta, J. A., Awschalom, D. D., Peng, X. & Alivisatos, A. P. Spin coherence in semiconductor quantum dots. *Physical Review B* **59**, R10421-R10424 (1999).
93 Poolton, N. R. J., Davies, J. J., Nicholls, J. E. & Fitzpatrick, B. J. An ODMR investigation of silver doped ZnSe. *Journal of Crystal Growth* **72**, 336-341 (1985).
94 Katari, J. E. B., Colvin, V. L. & Alivisatos, A. P. X-ray Photoelectron Spectroscopy of CdSe Nanocrystals with Applications to Studies of the Nanocrystal Surface. *The Journal of Physical Chemistry* **98**, 4109-4117 (1994).

Supporting Information

Excitonic Pathway to Photoinduced Magnetism in Colloidal Nanocrystals with Nonmagnetic Dopants

Valerio Pinchetti[1], Qiumei Di[2], Monica Lorenzon[1], Andrea Cammellini[3], Mauro Fasoli[1], Margherita Zavelani-Rossi[3], Francesco Meinardi[1], Jiatao Zhang[2*], Scott A. Crooker[4*], Sergio Brovelli[1*]

[1] *Dipartimento di Scienza dei Materiali, Università degli studi di Milano-Bicocca, via Roberto Cozzi 55, I-20125 Milano, Italy*

[2] *Research Center of Materials Science, School of Materials Science and Engineering, Beijing Institute of Technology, Beijing 100081, P.R. China*

[3] *National High Magnetic Field Laboratory, Los Alamos, New Mexico 87545, United States*

*e-mail: sergio.brovelli@mater.unimib.it; crooker@lanl.gov.

Figure S1 – TEM Images and Size Analysis of Ag-doped CdSe NCs.

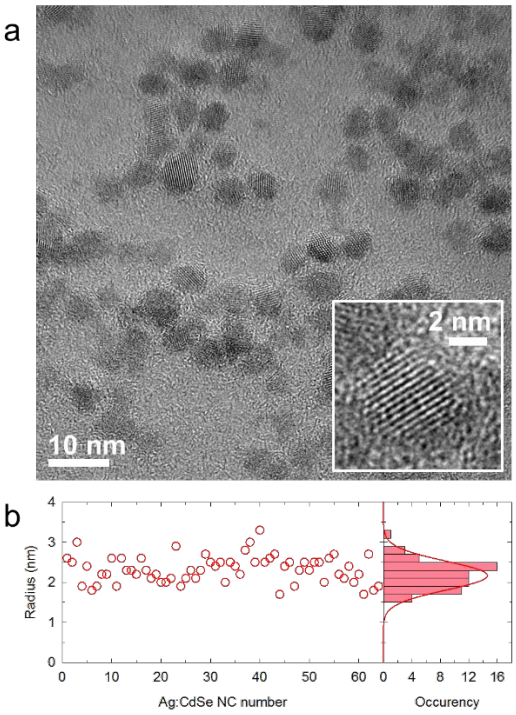

Figure S1 - (a**)** Transmission electron microscopy (TEM) image of an ensemble of Ag-doped CdSe NCs. The inset is a TEM image of a single NC. (b) Statistical analysis of the size of 65 Ag:CdSe NCs from the TEM image. The average size is 2.2±0.4 nm (red line).

Figure S2 – XRD Pattern of Ag:CdSe NCs.

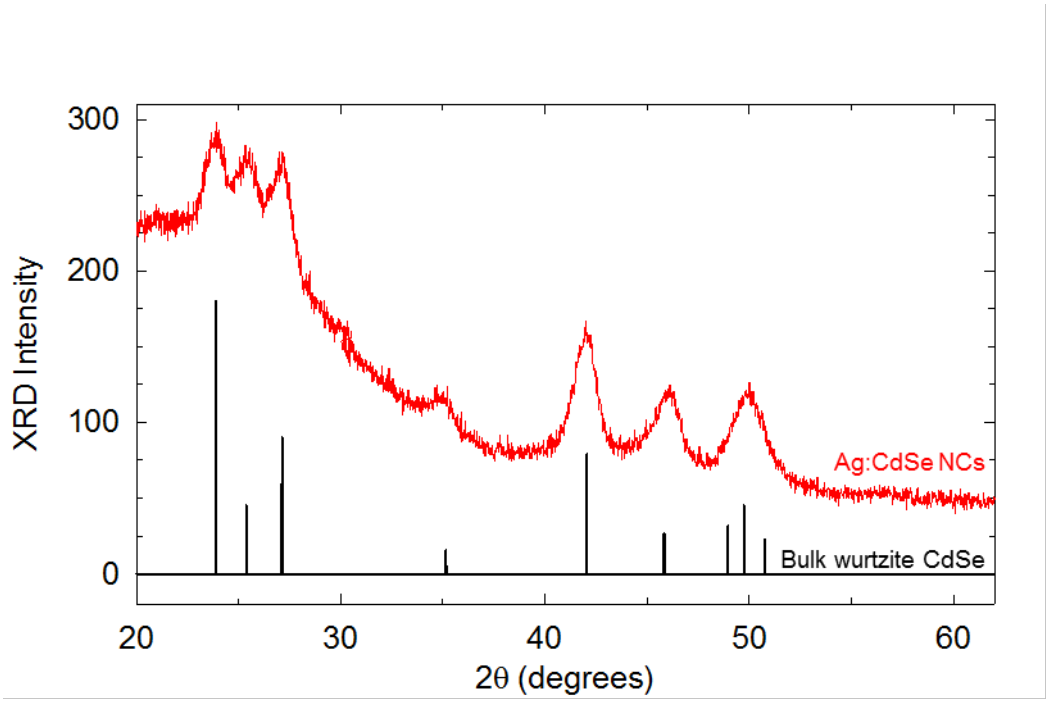

Figure S2 – X-Ray Diffraction (XRD) pattern of Ag:CdSe NCs (red line) together with the pattern of bulk CdSe in wurtzite phase (black line).

Figure S3 – XPS Spectra of Ag:CdSe NCs.

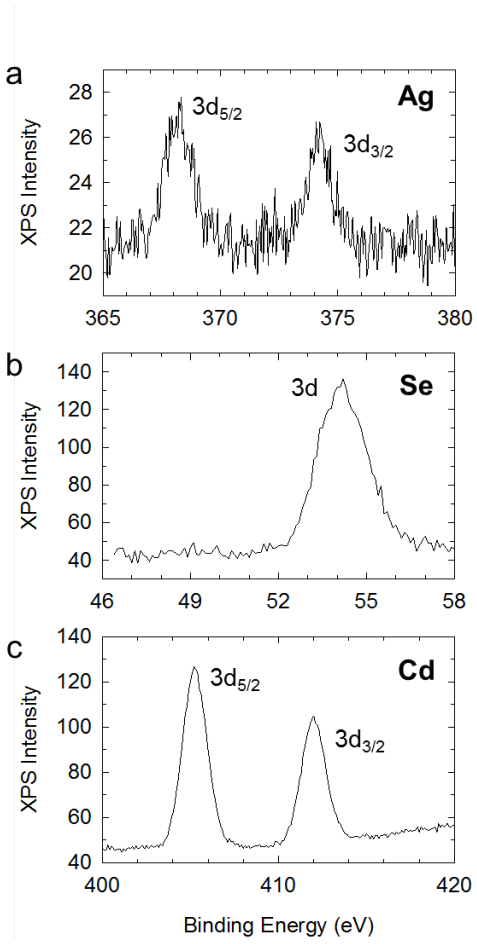

Figure S3 – X-Ray Photoelectron Spectroscopy (XPS) spectra of Ag:CdSe NCs for (a) silver, (b) selenium and (c) cadmium states.

To characterize the Ag concentration in our NCs, XPS on as-prepared CdSe QDs was carried out, as shown in Figure S3. The Cd3d peak is split into $3d_{5/2}$ (405.3 eV) and $3d_{3/2}$ (412 eV) peaks, and the peak at 54.2eV corresponds to Se 3d transitions. These observed binding energies are in agreement with reported data on CdSe NCs.[94] and confirm the intrinsic CdSe lattice framework .The clear Ag3d peaks in Figure S3a and the corresponding atomic concentrations in Table S1 confirm the existence of Ag^{+} dopant with 3% concentration (according to the fitting results of the $Ag3d_{5/2}$ and $Ag3d_{3/2}$ peaks).

Figure S4 – Double exponential fit of the Ag^+ TA kinetics under BE excitation

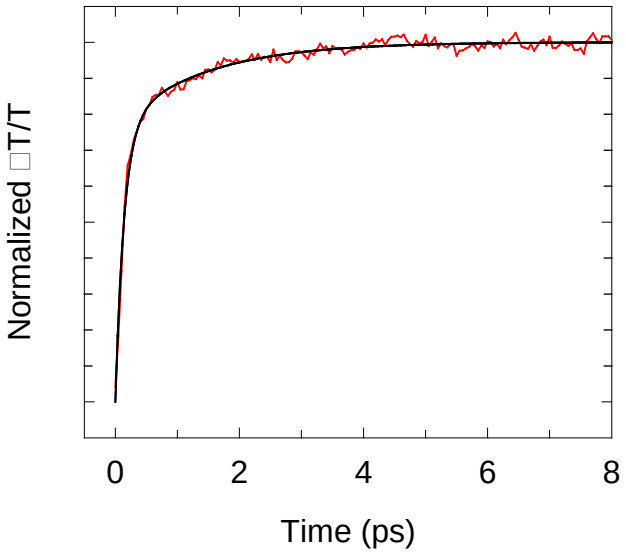

Figure S4. Normalized bleaching ΔT/T kinetics of the Ag^+ absorption (1.9 eV, red line) upon pumping close to the band-edge at 2.3 eV. The fitting curve to a double exponential function is shown as black line. The fitting (χ^2=0.9860) yields an 'instantaneous' component with ~140 fs risetime, close to the resolution limit of our experiment, and a 'slow' rise with time constant of 1.4 ps ascribed to the localization of the VB hole in the Ag^+ site.

Figure S5 – Reproducibility of the SEC response of Ag:CdSe NCs under negative V_{EC}

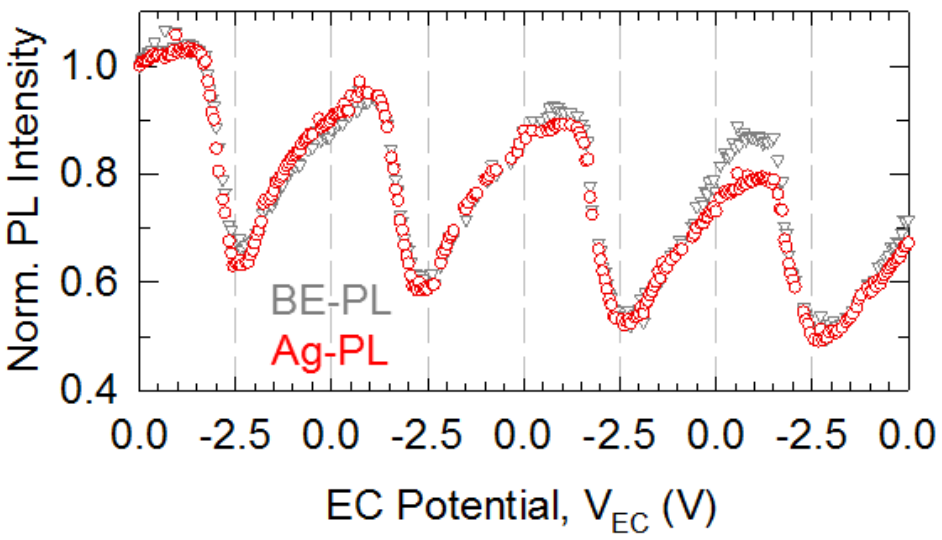

Figure S5 – Integrated BE-PL and Ag-PL (grey triangles and red circles respectively) intensities during 4 EC cycles, starting from V_{EC} = 0 V down to V_{EC} = -2.5 V.

Table S1 – Elemental Analysis of Ag:CdSe NCs by XPS Spectra.

	Atomic concentration (Cd 3*d*,)	Atomic concentration (Se 3*d*, %)	Atomic concentration (Ag 3*d*, %)
Ag:CdSe NCs	55.2%	41.8%	3%

Table S1 – Relative atomic concentrations of Cd, Se and Ag in Ag-doped CdSe NCs calculated using the XPS data reported in Figure S3.